Available online at www.sciencedirect.com
SCIENCE DIRECT®
Journal of Power Sources 118 (2003) 86–95
JOURNAL OF POWER SOURCES
www.elsevier.com/locate/jpowsour

Efficient simulation of fuel cell stacks with the volume averaging method

M. Roos[a,*], E. Batawi[b], U. Harnisch[a], Th. Hocker[a]

[a] *University of Applied Sciences Winterthur, P.O. Box 805, CH-8401 Winterthur, Switzerland*
[b] *Sulzer Hexis Ltd., P.O. Box 414, CH-8401 Winterthur, Switzerland*

Abstract

In fuel cell systems, a multitude of coupled physical and chemical processes take place within the assembly: fluid flow, diffusion, charge and heat transport, as well as electrochemical reactions. For design and optimisation purposes, direct numerical simulation of the full three-dimensional (3D) structure (using CFD tools) is often not feasible due to the large range of length scales that are associated with the various physical and chemical phenomena. However, since many fuel cell components such as gas ducts or current collectors are made of repetitive structures, volume averaging techniques can be employed to replace details of the original structure by their averaged counterparts. In this study, we present simulation results for SOFC fuel cells that are based on a two-step procedure: first, for all repetitive structures detailed 3D finite element simulations are used to obtain effective parameters for the transport equations and interaction terms for averaged quantities. Bipolar plates, for example, are characterised by their porosity and permeability with respect to fluid flow and by anisotropic material tensors for heat and charge transport. Similarly one obtains effective values for the Nernst potential and various kinetic parameters. The complex structural information is thereby cast into effective material properties. In a second step, we utilise these quantities to simulate fuel cells in 2D, thereby decreasing the computation time by several orders of magnitude. Depending on the design and optimisation goals, one chooses appropriate cuts perpendicular or along the stack axis. The resulting models provide current densities, temperature and species distributions as well as operation characteristics. We tested our method with the FEM-based multiphysics software NMSeses, which offers the flexibility to specify the necessary effective models. Results of simulation runs for Sulzer HEXIS–SOFC stacks are presented.

Keywords: Fuel cell simulation; Volume averaging; FEM; Multiphysics simulation

1. Introduction

Fuel cells (FCs) have the ability to directly convert hydrogen or hydrocarbon fuels to electricity and heat using electrochemical reactions. Hence, they represent an efficient and environmentally friendly alternative to traditional combustion processes. The commercial potential of fuel cells for use, for example, in automotive applications, residential co-generation, or portable consumer electronics, has been recognised for many years. However, only in recent years major technical barriers have been overcome so that FC technology now has become a major industrial trend.

The recent transfer of R&D activities from universities to companies shifted the main focus from demonstration of new materials and principles to the development of reliable and cost-effective products for mass market applications. This trend also has an impact on the numerical modelling of FC devices. Companies are now in need of effective simulation tools to speed up their development processes. However, since fuel cells are complex devices with a multitude of tightly coupled physical and chemical phenomena taking place, it is clear that there is no simple simulation tool ready to satisfy all these demands. Rather, tools are needed with a high degree of flexibility to combine submodels of different complexity (incorporating, for example, effects occurring at different length scales) to larger units. As an example, consider the close interrelation of the generation of electric energy at the triple phase boundary with the release of heat due to reversible and irreversible processes. This happens on a microscopic level. However, heat has to be removed over large distances to guarantee optimal operation. Furthermore, heat removal must not ruin the electrical performance, e.g. due to large amounts of excess air in the cathode compartment for cooling purposes or by the need of additional cooling fluids.

Another feature of fuel cells systems is their hierarchical arrangement of many similar or identical substructures: a FCstack consists of cells, which themselves are composed of many similar flow-field structures (meanders, nipples, etc.). This enables one to perform simulations of the smallest repetitive structures present and to characterise their behaviour

* Corresponding author. Tel.: +41-52-267-7797; fax: +41-52-267-7781.
E-mail address: markus.roos@zhwin.ch (M. Roos).

0378-7753/03/$ – see front matter © 2003 Elsevier Science B.V. All rights reserved.
doi:10.1016/S0378-7753(03)00066-1

through effective transport parameters such as average permeabilities and average thermal conductivities.

These detailed submodels are then included into higher-level models as geometrically uniform materials with the same characteristics. This approach is especially efficient when a complex three-dimensional (3D) geometry can be mapped onto a two-dimensional (2D) domain.

In this study, we present such an approach to simulate FCs, namely the numerical volume averaging method (NVAM), which is based on the volume averaging method (VAM) [1] and the theory of macro transport equations (MTE) [2]. On the one hand, this approach is much more efficient than the more traditional use of CFD codes that relies on the full discretisation of structural details [3]. NVAM enables the abstraction of a (part of a) complex geometry. On the other hand, NVAM is rigorously based on the governing balance and constitutive equations of continuum physics, i.e. it is not necessary to assess FC behaviour by system identification tools using a black box approach. Therefore, NVAM is able to bridge the gap between numerical simulation on a first principles level and a pure system dynamics modelling approach.

2. Averaged transport equations

To illustrate our approach we consider as an example the mass transport in porous media. The term *porous* is used in a wide sense, here we consider the gas diffusion in an SOFC electrode as well as the flow field in millimetre range channels as *porous flow*. The method then can be generalised to additional transport phenomena of interest in FC modelling, including heat and charge transport, etc.

2.1. The volume averaging method

The volume averaging method (VAM) was developed to describe transport phenomena in ordered or disordered porous media [1]. The existence of at least two different length scales is characteristic for these media: the typical diameter of the pores and the device length, as shown in Fig. 1. The actual transport process takes place in the void space defined by the pores. The governing equations are due to Navier–Stokes, i.e.

$$\vec{\nabla}(\rho\vec{v}\otimes\vec{v}) = -\vec{\nabla}P + \vec{\nabla}\cdot\vec{\vec{\tau}}$$
$$\tau_{ij} = \mu(\partial_i v_j + \partial_j v_i) - \tfrac{2}{3}\mu(\vec{\nabla}\cdot\vec{v})\delta_{ij}, \quad (1)$$

with the pressure P, the fluid density ρ, the viscosity μ, and the stress tensor τ. These quantities are defined only *within* the pores. Eq. (1) are virtually intractable numerically for many technically important structures due to the complex geometry and the immense effort to specify a computational grid and the boundary conditions for a piece of, e.g. a porous ceramic material.

The solution to this problem is the description of physically relevant fields only on an average basis. The approach given in [1] deduces effective transport equations for suitably defined volume averages of the true physical quantities: the averaged velocity field is defined by

$$\vec{v}_{\mathrm{av}} \equiv \frac{1}{V_\Omega}\int\int\int_\Omega \vec{v}(\vec{x})\mathrm{d}V, \quad (2)$$

where Ω denotes an averaging volume that is large with respect to the pore length scale, but small compared to the device length. V_Ω is the volume of Ω. After a lengthy calculation one finds a modified transport equation for the *averaged* velocity field together with an updated expression for the stress tensor τ_{eff}

$$-\vec{\nabla}P + \vec{\nabla}\cdot\vec{\vec{\tau}}_{\mathrm{eff}} - \frac{\mu}{k}\vec{v}_{\mathrm{av}} = 0, \quad (3)$$

where k denotes the *permeability* of the porous material. Usually the term involving the stress tensor is negligible compared to the last one, leading after rearrangement to

$$\frac{\mu}{k}\vec{v}_{\mathrm{av}} = -\vec{\nabla}P \quad (4)$$

the well-known Darcy equation. This equation applies to the whole domain of the device, i.e. there is no longer a need to formulate boundary conditions within the pores or to discretise the pore geometry as the averaged velocity field is continuous across the whole domain. The quantity k, which is a tensor of rank two in general, now contains the information about the pore geometry and expresses an anisotropy due to, e.g. an alignment of the pores along a characteristic direction of the material.

The challenge in applying VAM to transport problems is the solution of the so-called closure equations [1], which implicitly define the effective parameters characterising the porous material, (μ/k in Eq. (4)). The closure is a partial differential equation with at least the same complexity as the original transport equation. It has to be solved on a representative region of the porous medium using suitable boundary conditions. Sometimes it is possible to deduce certain properties of the effective parameters using analytical methods, but this rarely leads to actual figures for the transport parameters.

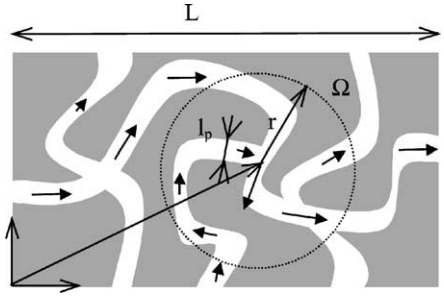

Fig. 1. Length scales in a porous medium: L, device length scale, l_p pore diameter. The radius r of the averaging volume has to satisfy the relation $l_p \ll r \ll L$.

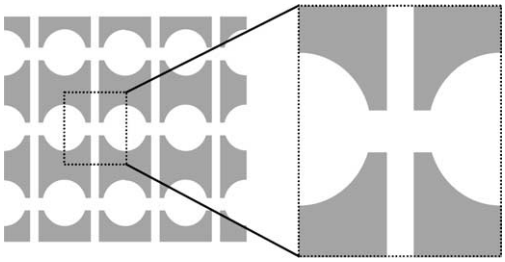

Fig. 2. Periodic porous structure and a possible elementary cell.

2.2. The macro transport equation method

In [2], a slightly different approach is outlined to deal with transport in porous media:[1] instead of starting with the definition of volume averages for the relevant quantities and deducing their transport equations, so-called macro transport equations (MTE) are set-up. These equations allow for the calculation of the physical quantities at suitably chosen reference points. The method is ideal for ordered materials, but also applies with certain restrictions to disordered materials.

One of the critical issues with this method is the determination of the effective transport parameters. Again one has to solve specific abstract PDEs on elementary cells on a periodic domain, cf. Fig. 2.

2.3. The numerical volume averaging method

To simplify the application of either VAM or MTE one has to avoid the solution of the closure PDEs. Instead of doing abstract mathematics, we perform *virtual experiments* on a repetitive region of the porous medium using a computer simulation code to obtain the effective parameters, as shown in Fig. 3. With suitable boundary conditions on this domain we are able to ''measure'' the tensor components of the permeability tensor k, i.e. k_{xx} and k_{yy}. This is, of course, reminiscent to the work of an experimentalist, who does exactly the same thing in reality to confirm Darcy's law for a given material. He sets up a pressure gradient in a chosen direction, measures the corresponding flow rates in all possible directions, and extracts the material properties in tensor form.

Although NVAM still is based on the solution of PDEs on complex domains, it has a number of advantages over its parent methods:

- There is no need to implement specific closure PDEs as in VAM to get effective parameters. One uses the given, well known transport equations with their clear physical interpretation.

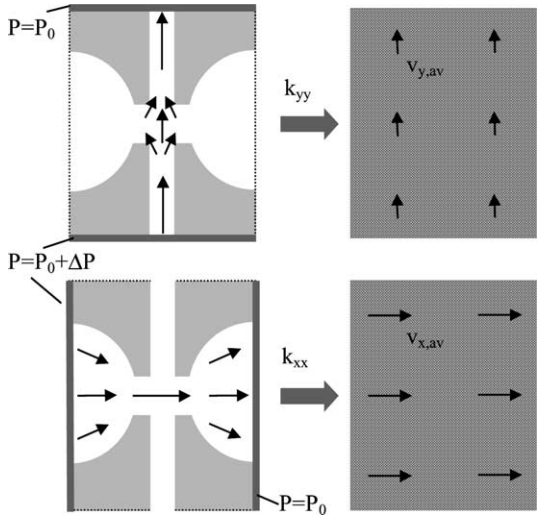

Fig. 3. NVAM for a complex pore structure showing anisotropic behaviour: calculation of k_{xx} (top) and of k_{yy} (bottom). Solid lines indicate the driving boundary conditions for the flow, while on the remaining boundaries the no-flux condition applies.

- There exists a multitude of commercial and non-commercial numerical simulation tools that already perform the necessary calculations.
- With the analogy to experimental work and the physical interpretation of the necessary simulations, it is possible to apply NVAM to virtually any transport phenomenon.
- NVAM also works for complex material behaviour found in many engineering applications. Consider, e.g. the case, where mass transport occurs in non-isothermal states. While VAM in its basic formulation is not applicable because isothermal behaviour is assumed, NVAM still works: one performs the virtual experiment simply by *including* the given thermal gradient.[2]
- Moreover, it is possible to extend the approach to more complex situations, where transport processes take place in conjunction with chemical reactions. While the generalisation of VAM or MTE is complex, there is a straightforward generalisation in terms of NVAM.
- VAM or MTE are used to rigorously deduce the *form* of the effective transport equations, while NVAM provides a framework for efficient calculations for engineering tasks.

2.4. Numerical algorithms

In principle any numerical discretisation scheme could be adopted for the actual solution of mass transport or diffusion equations, etc. The most prominent example is the finite volume method in conjunction with an explicit time integration scheme. Another choice is the finite element method (FEM), suitable especially for stationary states. We have

[1] The macro transport equation method is, in fact, much more general and allows also for the simplification of transport equations if the simulation domain contains a direction with reduced complexity, e.g. a slit.

[2] However, it is no longer guaranteed that the form of the effective transport equation still remains valid. This could be proven only by regress to the traditional approach, i.e. VAM.

used this method because it provides the highest flexibility to simulate complex material behaviour and boundary conditions. Through the volume averaging process, all the information about the geometrical structure is cast into the anisotropy of the effective parameters. For layered media, for example, different values of the thermal conductivity in or transversal to the layer result [2]. Anisotropic material behaviour can easily be adopted in finite element formulations. The same is true for complex interaction models, which arise, e.g. by averaging the electrochemical kinetics over electrode and electrolyte domains. As a result, the phenomenological kinetics depend on the current density due to mass transport limitations through the porous electrode.

2.5. Application to fuel cell structures

We applied NVAM to fuel cell simulations. This is of great interest since a typical fuel cell device contains at least four different length scales rendering numerical simulations especially cumbersome. These are (with an example of the dominant effect):

- Nanopore scale (from 10^{-7} to 10^{-8} m): chemical reactions occurring at the triple phase boundary.
- Porous material scale (from 10^{-5} to 10^{-6} m): diffusion transport in ceramic electrodes.
- Flow channel scale (from 10^{-3} to 10^{-4} m): free fluid flow together with diffusion.
- Device scale (from 10^{0} to 10^{-2} m): cells and stacks operation, including the balance of plant.

Of course, it is impossible with desktop computers to cover this range of length scales within a single numerical scheme. The macro transport equations approach can serve as a generic method to tackle this issue. One starts from the physical description level and develops a cascade of macro transport equations: each level's transport equations are parameterised by models of the next lower level. Put into action, this scheme works out as follows for SOFC simulation:

- A 3D model of the micropores at the electrode–electrolyte interface provides effective kinetic models for the electrochemical processes at the next higher level.
- A 3D model of a representative part of a MIC/electrode/electrolyte/MIC structure is used to obtain effective transport parameters for fluid transport at the flow channel scale in the MIC.
- A 2D model of the cell (or the stack) is set-up. To describe fluid flow, the MIC is modelled as a macroporous structure.
- Stacking of several cell models allows for the simulation of whole stacks.

It is possible to combine this approach with experimental data at any level. If the lowest level is omitted, missing information can be taken from experimental work, e.g. impedance spectroscopy to access the basic parameters of the electrochemical kinetics. This is often necessary, as the elementary chemical reactions are rarely known. At any level, the experimental data can be used to validate NVAM results.

2.6. Lateral models

The typical geometry of flow fields in PEFC cells is truly three-dimensional. With approximate 2D models of these structures, some relevant interactions or geometric influences have to be discarded. NVAM provides a novel approach to this issue: a lateral 2D cell model is specified by adopting suitable macro transport equations for an averaged flow field. The omitted third dimension (z-direction in Fig. 4) manifests itself in various ways: the viscous friction with the upper and lower walls is absorbed into the permeability tensor. Averaging according to NVAM provides the anisotropic tensor for the permeability. In-plane heat transfer is also described by anisotropic material tensors. Heat and/or charge transport to neighbouring cells in the transverse (z-direction) is accounted for by setting up suitable interaction models, e.g. a temperature dependent heat source to reflect Newton-type cooling.

The electrochemical reactions (taking place at an interface between layers) are described in a lateral model by an effective 2D volume reaction. A detailed 3D submodel similar to, e.g. the one presented in [4] for PEFC processes, provides effective parameters. Geometric effects, properties of the MEA, transversal diffusion in the gas channels, etc. is accounted for by complex kinetic equations, to be parameterised with help of the 3D submodel.

Due to the reduction of complexity by using a 2D lateral model, localised effects, such as the formation of hot spots, cannot be studied in this way. Only phenomena on the length scale of the averaging process used in NVAM can be addressed.

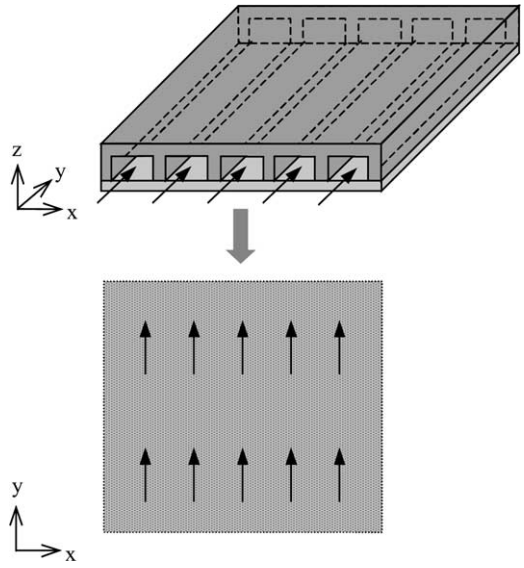

Fig. 4. The 3D flow-field structure and its representation in a 2D lateral model with anisotropic material behaviour.

2.7. Concluding remarks

The description of the NVAM closes with some remarks about this method:

- The application of the method to actual devices is straightforward, as it does not depend on complex mathematical derivations or the need for an implementation of unfamiliar abstract PDEs.
- NVAM models can be tailored to fit to engineering tasks. The researcher decides on the degree of complexity necessary to tackle the actual problem, while keeping the computational costs low.
- It is possible to introduce experimental data at any levels of the modelling hierarchy, thereby replacing the lower levels or validate the numerical model.
- NVAM interpolates from the pure scientific approach with its ab initio transport process formulation up to the pure engineering task of black box modelling.
- Application of NAVM exhibits a strong analogy to experimental work. In fact, this modelling approach is best described as *performing virtual experiments*. It is hoped that it will be accepted more easily by development engineers than more abstract numerical schemes.

3. Application to SOFC modelling

We tested the NVAM by simulating solid oxide fuel cells and stacks with the HEXIS[3] design [5–7]. This system exhibits a high integration level, as heat exchange, fuel reforming, electrochemical reactions and after burning take place within a single housing. The design of the stack asks for careful optimisation to meet the (often) conflicting goals. This can be done efficiently only with help of detailed numerical simulations because many processes strongly interact. Due to the geometrical complexity of the real structure, only a method like NVAM can support engineering tasks at affordable costs [7].

To set-up a single cell model, we started from the second-lowest level (macroporous scale) because there is no detailed information on the nano scale available. On any stage, the relevant set of PDEs describing the transport phenomena have to be solved. The following set of independent fields has been used: temperature T, velocity field $\vec{v}$, pressure P, molar fractions x_α for each species out of the set $\alpha \in \{H_2, H_2O, O_2, N_2, CO, CO_2, CH_4\}$, and the electric potential Φ.

3.1. Transport equations for SOFC systems

The governing law for fluid flow in void regions are the Navier–Stokes equations, Eq. (1), which apply to the flow-field regions of a 3D model of the MIC, or to the piping. The ideal gas law links the mass density to the species molar fractions, pressure and the local temperature by

$$\rho = \frac{P}{RT}\sum_\alpha x_\alpha M_\alpha, \tag{5}$$

with the universal gas constant R, the molar masses M_α and the molar species fractions x_α. Of course, more complex constitutive laws for the fluid are feasible, but the ideal gas law describes the behaviour of high temperature gases very well. In porous media, e.g. within the ceramic electrodes or in 2D representations of 3D flow fields, we adopt Darcy's law (Eq. (3)).

In any case, one has to combine Eq. (1) or Eq. (2) with the continuity equation, i.e. the mass balance reading for stationary states

$$\nabla \cdot (\rho\vec{v}) = 0. \tag{6}$$

The diffusion equation for species transport in void and porous materials reads

$$\vec{\nabla} \cdot (\rho_\alpha \vec{v}) = -\vec{\nabla} \cdot \vec{j}_\alpha + \Pi_\alpha, \tag{7}$$

where the mass density for species α is given by $\rho_\alpha = x_\alpha M_\alpha c$ and the molar concentration equals $c = \rho\left(\sum_\alpha x_\alpha M_\alpha\right)^{-1}$. Π_α denotes the production rate of species α (based on the mass density). This rate is the sum of all active chemical reactions, i.e.

$$\Pi_\alpha = \Pi_\alpha^{\mathrm{QH}} + \Pi_\alpha^{\mathrm{TPB}}, \tag{8}$$

The first term is the contribution of all homogenous and quasi homogenous reactions, e.g. the reforming and shift reactions in the Ni-cermet anode of a SOFC system and reads $\Pi_\alpha^{\mathrm{QH}} = M_\alpha \sum_n \nu_{\alpha n} r_n$, where $\nu_{\alpha n}$ is the stoichiometric coefficient for species α in reaction n and r_n the molar reaction rate density for reaction n. This last quantity has to be supplied according to the catalytic properties of the given material. Of course, the rate densities usually depend on the local temperature, species concentrations, etc. The second term on the RHS of Eq. (8) represents the contributions of the electrochemical reactions at the triple phase boundary (TPB). Their form will be discussed later.

The species diffusion current density (measured with respect to the centre of mass system), finally, reads

$$\vec{j}_\alpha = -\sum_\beta \frac{c^2 M_\alpha M_\beta}{\rho}\hat{D}_{\alpha\beta}\vec{\nabla}x_\alpha, \tag{9a}$$

where Stefan–Maxwell's law implicitly defines the effective diffusion constants $\hat{D}_{\alpha\beta}$ by

$$\vec{\nabla}x_\alpha = -\sum_\beta \frac{1}{cD_{\alpha\beta}}\left(\frac{x_\alpha\vec{j}_\beta}{M_\beta} - \frac{x_\beta\vec{j}_\alpha}{M_\alpha}\right), \tag{9b}$$

The latter expression depends on the binary diffusion coefficients $D_{\alpha\beta}$, which are functions of temperature and

[3] The acronym HEXIS corresponds to heat exchanger integrated stack, a SOFC concept developed by Sulzer AG, Switzerland.

pressure. In microporous regions, the binary diffusion coefficients are further scaled to account for the effect of pore diffusion (Bruggemann correction). The effective value reads then

$$D_{\alpha\beta,p} = \varepsilon^{1.5} D_{\alpha\beta}, \tag{10}$$

where ε denotes the (volumetric) porosity. The heat transport equation applies to all simulation domains (with vanishing convective contributions in solid materials, of course)

$$\vec{\nabla} \cdot \left(\sum_{\alpha} h_\alpha \rho_\alpha \vec{v} \right) = -\vec{\nabla} \cdot \vec{j}_{th} - \vec{\nabla} \cdot \sum_{\alpha} h_\alpha \vec{j}_\alpha + \Pi_{\text{th}}, \tag{11}$$

where h_α is the (mass density based) enthalpy of species α, approximated for ideal gases by $h_\alpha = c_{p,\alpha} T$. The heat production rate Π_{th} is given by

$$\Pi_{\text{th}} = \sum_{n} \Pi_{\text{th},n}^{\text{QH}} + \sum_{s} \Pi_{\text{th},s}^{\text{TPB}} + \Pi_{\text{th,el}} + \Pi_{\text{th,ext}}, \tag{12}$$

where the first term on the RHS corresponds to the heat release of the quasi-homogenous reactions. We set $\Pi_{\text{th},n}^{\text{QH}} = -\Delta H_n r_n$ with ΔH_n denoting the reaction enthalpy for reaction n and r_n the corresponding rate. The second term corresponds to the electrochemical reactions, see Section 3.2.

The third term, $\Pi_{\text{th,el}} = \sigma^{-1} |j_q|^2$, is due to Joule's heating with the material's electric conductivity σ and the electric charge–current density j_q. The term $\Pi_{\text{th,ext}}$ accounts for an external heat source or sink due to cooling mechanisms or—for 2D lateral models—accounts for heat–currents directed into the omitted third direction, cf. remarks at the end of Section 2.7.

Finally, the heat–current density reads according to Fourier's law of heat conduction

$$\vec{j}_{\text{th}} = -\lambda \vec{\nabla} T. \tag{13}$$

The thermal conductivity λ might depend on local species concentrations, temperature and is in general a tensor quantity as explained in Section 2.

The charge transport equation, defined only in electrically conducting materials reads

$$-\vec{\nabla} \cdot \vec{j}_q + \sum_{s} \Sigma_s^{\text{TPB}} = 0, \tag{14}$$

where Σ_s^{TPB} represents the (singular) charge double layer, cf. Section 3.2. The charge–current density $\vec{j}_q$ is given by the microscopic version of Ohm's law

$$\vec{j}_q = -\sigma \vec{\nabla} \Phi, \tag{15}$$

where σ denotes the electric conductivity in MIC and electrode regions and the ionic conductivity in the electrolyte region. It is well known that the ionic conduction in solid oxide electrolytes can be approximated by Ohm's law [10] (in contrast to liquid or polymer electrolytes).

3.2. Implementation of the electrochemistry

In addition to (quasi) homogenous reactions in the porous electrodes or void spaces, one has to describe the electrochemical reactions. SOFC systems are able to electrochemically oxidise hydrogen as well as carbon monoxide directly. The overall reactions reads

$$2H_2 + O_2 \Rightarrow 2H_2O, \tag{16a}$$

and

$$2CO + O_2 \Rightarrow 2CO_2, \tag{16b}$$

The actual reactions at the anode triple phase boundary are given by

$$2H_2 + 2O^{2-} \Rightarrow 2H_2O + 4e^- \tag{17a}$$

and

$$2CO + 2O^{2-} \Rightarrow 2CO_2 + 4e^- \tag{17b}$$

while the process at the cathode TPB reads

$$O_2 + 4e^- \Rightarrow 2O^{2-}. \tag{18}$$

These reactions contribute to the source terms in the charge, species and heat transport equations. The source term for charge transport reads

$$\Sigma_s^{\text{TPB}} = \Delta\Psi_s \vec{n} \vec{\nabla} (\delta(f) \cdot |\vec{\nabla} f|), \tag{19}$$

where the scalar function $f(\vec{x}) = 0$ defines the location of the TPB interface in space. $\Delta\Psi_s$ denotes the (irreversible) potential jump across the TPB for reaction s and is given by

$$\Delta\Psi_s = \Delta\Psi_s^0 - \frac{\vec{j}_{q,s} \cdot \vec{n}}{g_s}, \tag{20}$$

where $\Delta\Psi_s^0$ denotes Nernst's potential at thermodynamic equilibrium for reaction s (cf. Eq. (24)), g_s is the double layer surface conductance, which is used to model the activation overpotential, cf. Eq. (25), and $\vec{j}_{q,s}$ finally corresponds to the current density across the TPB due to reaction s.

The additional contributions to the source terms for heat and species transport can be expressed with help of the reaction rate per unit area at the TPB

$$r_s^{\text{TPB}} = \frac{(\vec{j}_{q,s} \cdot \vec{\nabla} f) \delta(f)}{n_s F}, \tag{21}$$

where n_s corresponds to the number of electrons transferred in reaction s and F is Faraday's constant. The source term in Eq. (12) due to electrochemistry reads then

$$\Pi_\alpha^{\text{TPB}} = M_\alpha \sum_{s} \nu_{\alpha,s} \cdot r_s^{\text{TPB}}, \tag{22}$$

where $\nu_{\alpha,s}$ is again the stoichiometric coefficient. The contribution to the heat balance is given by

$$\Pi_{\text{th}}^{\text{TPB}} = -T \sum_{s} \Delta S_s r_s^{\text{TPB}} + \sum_{s} g_s^{-1} |\vec{n} \cdot \vec{j}_{q,s}|^2 \delta(f) |\vec{\nabla} f|, \tag{23}$$

where ΔS_s denotes the entropy release in reaction s (reversible release of heat) and the second term corresponds to losses due to irreversible processes, i.e. the activation losses.

The expression for Nernst's potential for reaction s at thermodynamical equilibrium reads

$$\Delta\Psi_s^0 = \frac{\Delta H_s - T\Delta S_s}{n_s F} - \frac{RT}{n_s F}\sum_\alpha \nu_{\alpha,s}\ln(x_\alpha), \tag{24}$$

where the first term corresponds to Nernst's potential at normal conditions and the second contribution accounts for the change of the activity in the actual state. If there is more than one electrochemical reaction present (e.g. the oxidation of CO in the solid oxide fuel cell) the actual potential jump at the TPB is determined by the competing reactions. Even for zero net current density across the electrolyte, there might be non-zero rates for the individual reactions. It is assumed here, that they interact only via their contribution to the total potential jump, but can be treated independently otherwise.

The activation overpotential at cathode or anode is implicitly defined through the surface conductance [8] and reads

$$g_s = k_s\left(x_\alpha\frac{P}{P_{\text{ref}}}\right)^{m_s}\frac{2F}{RT}e^{-(E_{\text{act},s})/(RT)}. \tag{25}$$

Here k_s denotes a phenomenological pre-exponential factor for reaction s, $E_{\text{act},s}$ its the activation energy, P_{ref} a reference pressure, and m_s an exponent describing the activation kinetics. This corresponds to a linearisation of the Butler–Volmer equation and is well justified for SOFC conditions [8].

3.3. Solution method

The set of partial differential equations, i.e., Eqs. (1) or (4), (6), (7), (9a), (9b), (11), (13)–(15) have been implemented in the FE-based code NMSeses [9]. Most material and process properties can be accessed on the user level, i.e. material temperature dependencies, kinetic laws, etc. can be freely defined.

Due to the strong non-linear dependencies in the expressions for the reaction rates and some of the material properties, the FE-tool allows for the specification of partial derivatives (with respect to the independent fields) to speed up the convergence rate.

Grouping the independent fields into two or more solution field blocks can further optimise the convergence behaviour. The fields within a given block are solved by the Newton–Raphson algorithm, which converges quadratically if the initial starting solution is carefully chosen and the partial derivatives w.r.t. all block fields are defined.

The algorithm implemented in NMSeses solves the given blocks consecutively until overall convergence is obtained. This is usually fast, if an optimal block structure has been defined. Best convergence properties have been found with a two-blocks choice: Block1 = {velocity, pressure} and Block2 = {species molar fractions, temperature, electric potential}.

The overall loop converges not exceeding 15 Newton–Raphson-iterations, taking typically <2 min computer time per SOFC operation point on an Athlon XP2000 (1.6 GHz) for the single cell model of Section 3.5. Therefore, a full performance plot is calculated in <2 h. The 3D models of Section 3.4 generally require more computer resources.

3.4. 3D model at macroporous level

3.4.1. Model specification

On the macroporous level, we used a 3D model for the domain shown in Fig. 5. It reflects the true geometry of the flow regions inside the MIC described by Eq. (1). For cathode and anode electrodes, the porous flow equation (Eq. (4)) is used. The material properties, i.e. porosity and permeability were taken from the literature [10], or fitted to experimental results if available, or estimated otherwise.

An important issue in applying NVAM is the specification of boundary conditions. This is straightforward for heat conduction or laminar flow: the symmetries of the device dictate the boundary conditions of the domain. We have used zero-flow conditions across the mirror planes, while planes perpendicular to the flow direction were modelled isothermal (or isobaric) with a given drop of temperature (or pressure) across the system.

Setting up the boundary conditions becomes more involved for systems where dispersion, i.e. the interaction of diffusive and convective transport (of heat or species) plays a major role. In this case, the boundary conditions are less obvious because there are fewer symmetries to use, as the *direction* of the convective current breaks one symmetry.

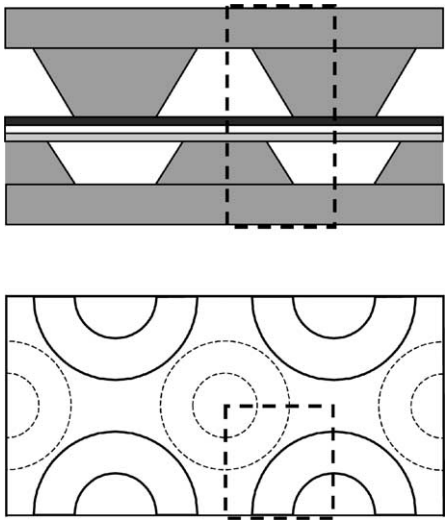

Fig. 5. Side (top) and horizontal (bottom) view of the metallic interconnect (MIC) structure. The repetitive element used for numerical simulation is indicated by the dashed lines.

This can be tackled by adopting generalised periodic boundary conditions. While the heat–current density (or the velocity flow) is periodic across the repetitive domain in flow direction, the corresponding potential field, i.e. temperature (or pressure) consists of a periodic part plus a superimposed linear ramp [2]. In the parameter range for the actual simulations, we were able to estimate the transport parameters for heat and fluid flow independently, neglecting dispersion.

To date no simulations with electrochemical reactions have been performed with the 3D model shown in Fig. 5. While such calculations are of great interest to predict the net efficiency of the energy conversion and their dependence on geometry, it is mandatory to have independent measurements of the *local* properties of the electrochemical interactions. Since so far only IV-curves for full cells are available, no direct comparison of NVAM and experiment is possible.

3.4.2. Results for the 3D model

We calculated the permeability for the flow fields in the MIC structure for the anode and cathode, as well as the heat and charge conductivities. Unfortunately, there are no independent measurements for these transport parameters available. Nevertheless, the numerical simulations still provide important insight: one is able to estimate trends if the geometrical structure is changed under otherwise identical conditions. These trends are often much more reliable in comparison to the predictions of absolute values.

3.5. Effective 2D cell model

The transport parameters from the 3D submodel (see Section 3.4) were readily included into the rotational symmetric 2D model, see lower part in Fig. 6. The reaction properties have to be taken from experimental IV-curves with help of the Ansatz functions for SOFC electrochemistry, cf. Eq. (22).

3.5.1. Model specification

We have chosen a rotational symmetric domain to approximate the HEXIS cell. The process of NVAM (with an averaging volume large compared to the extension of the nipples) renders the MIC flow-field rotational symmetric. This is not true, however, for the after burning and the air inlet zones along the outer circumference. At the present stage we have to accept this approximation.

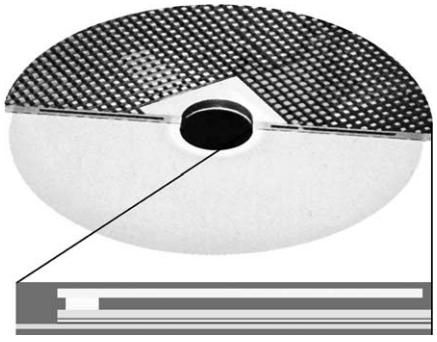

Fig. 6. The top view shows a part of a HEXIS–SOFC MIC, while the lower sketch depicts the corresponding 2D rotational symmetric FE model.

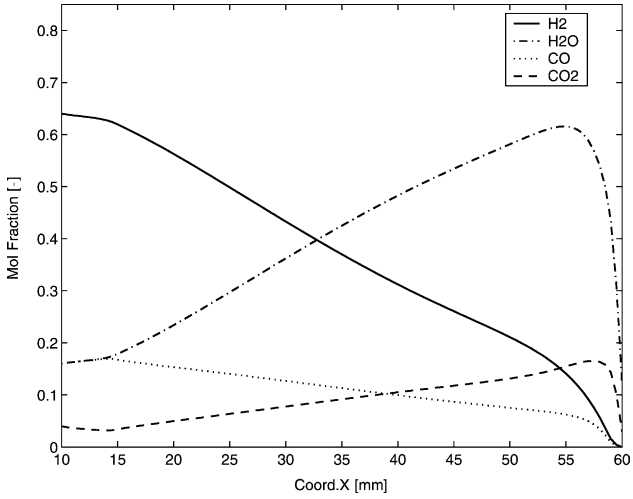

Fig. 7. Molar fractions for the species H_2, H_2O, CO and CO_2 along the radial coordinate of the 2D cell model shown in Fig. 6.

Fig. 7 shows the molar fractions of hydrogen, water, carbon monoxide, and carbon dioxide along the radial coordinate. The rather steep decrease of the gas components near 60 mm is due to the onset of the after-burning reaction and the diffusive mixing with the species of the air gas stream. Interpretation of these model properties under varying operation conditions, such as fuel mass flow, stack temperature, etc., is the key to improve the understanding of the internal states of SOFC cells. Since direct measurements of the gas composition inside the cell is very difficult, these results can be validated only indirectly, e.g. by comparing IV-curves or performance maps, cf. Section 3.5.2.

3.5.2. IV-Curves and performance maps

After the model calibration using a data set for a single value of the fuel mass flux, the model can be used to simulate the performance at different mass fluxes and external loads. In Fig. 8, a typical set of IV-curves is shown, for varying fuel mass fluxes.

This two-parameter set of results can be cast into so-called performance maps, Fig. 9. It shows lines of constant efficiency (solid lines), electrical power (dashed) and fuel utilisation (dashed–dotted). This information is plotted in a fuel mass flow versus voltage graph. The two graphs in Fig. 9 correspond to a thick electrolyte (top graph) and thin one (bottom), respectively. A comparison clearly demonstrates improved performance of the cell with the thinner electrolyte. Many more variations of the modelling conditions are feasible. The extraction of performance trends with

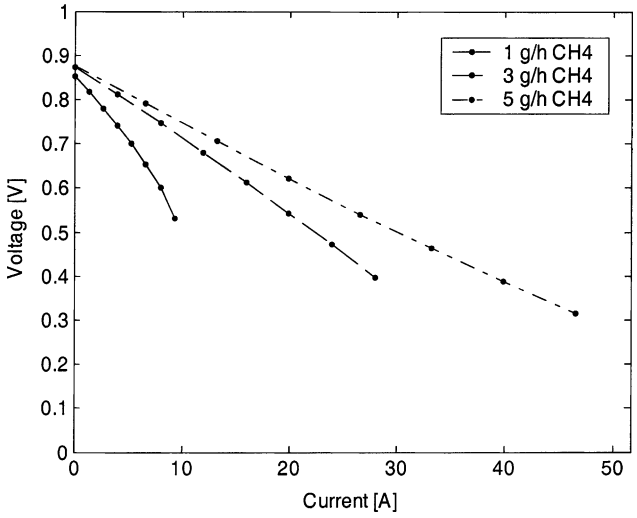

Fig. 8. IV-curves for different methane mass fluxes, 1 g/h (solid), 3 g/h (dashed) and 5 g/h (dashed–dotted).

respect to maximum power or efficiency help to improve a redesign of SOFC stacks.

3.6. System models

A further step in the modelling hierarchy addresses the system level. In order to maintain a nearly constant temperature throughout the stack at different operating conditions, the thermal insulation around the stack has to be able to dynamically adjust to the amount of heat released in the after-burning zone. This can be achieved through control of the air flow rate from the outside to the inside of the insulation and through effective heat-exchange between the cold air and the hot exhaust gases.

Fig. 10 shows the smallest repetitive structure of an arrangement of two insulation walls with an air gap in between. The walls are riddled so that air can flow in the direction opposite to the main heat flow, i.e. from outside to inside. Simulation of the temperature and flow fields then allows one to calculate the permeability and the thermal conductivity matrix of the 3D structure. With this information, the real structure can be replaced by a two-dimensional ''porous material'' with the same characteristics.

This is shown in Fig. 11, where the integrated air preheating and dynamic insulation of an SOFC system has been simulated in lateral direction. The outer thermal insulation has been modelled as a porous material with effective transport parameters that were obtained from the detailed 3D model shown in Fig. 10. Furthermore, details of the stack have been neglected here since for testing the performance of the insulation it is sufficient to specify the heat and mass fluxes in the after-burning zone around the stack. As a consequence, in such a highly optimised 2D model, typical calculations of the coupled pressure, velocities, and temperature fields only take few minutes so that optimisation tasks can be readily performed.

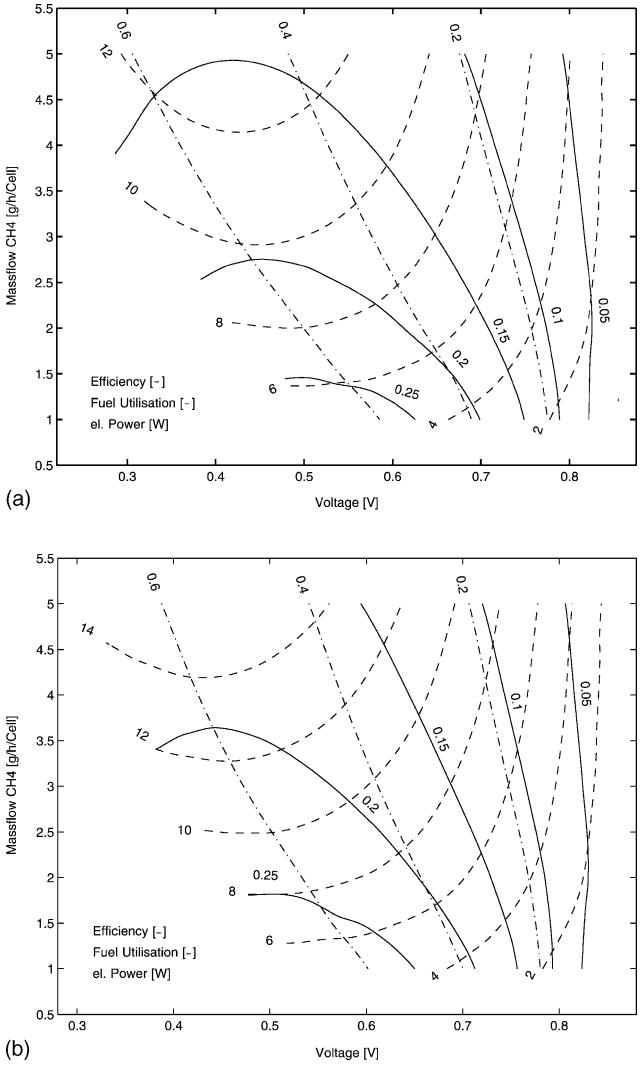

Fig. 9. Performance map for two cells, differing in the electrolyte dimension: thick (top graph) and thin (bottom graph). Lines of constant efficiency (solid), electrical power (dashed) and fuel utilisation (dashed–dotted) are shown. The figures for the current are given in A, while the others are dimensionless.

Results for the temperature distribution for the area enclosed by the dashed lines are presented in Fig. 12. While there are large temperature gradients within the heat exchange zone, the temperature becomes rather uniformly distributed further away from the stack.

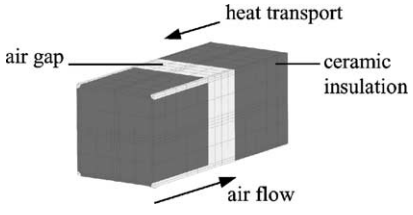

Fig. 10. The 3D model for the calculation of the transport properties of the thermal insulation structure.

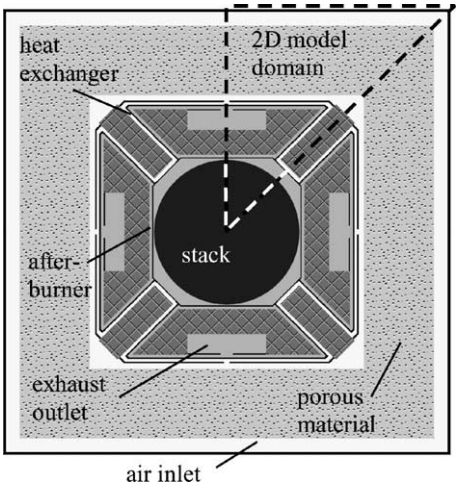

Fig. 11. The 2D cross-sectional model of a SOFC stack with integrated air pre-heating and thermal stack insulation. The cold air enters from the outer region, passing through the 3D structure depicted in Fig. 10 and enters the heat exchanger. The exhaust gas passes through the heat exchanger and exits through the outlets. The dashed triangle was modelled in 2D using a macro transport equation for the thermal insulation region.

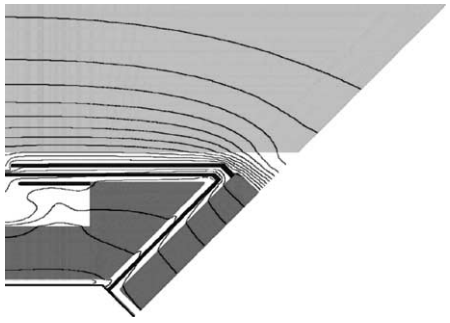

Fig. 12. Temperature distribution within the thermal insulation around the SOFC stack, calculated by a highly efficient 2D model. The shown area corresponds with the one enclosed by the dashed lines in Fig. 11.

4. Conclusions

4.1. Summary

We have presented a novel approach to the numerical modelling of fuel cells, stacks, and systems. The main feature of our approach is the adoption of macro transport equations to describe the relevant processes in terms of averaged physical quantities. The method of numerical volume averaging exhibits strong analogies to the work of experimentalists, in the sense that the determination of effective parameters can be described as performing virtual experiments.

It is possible in this way to abstract geometrical details of the system at hand and to absorb their influence into effective material properties. These parameters are often tensor quantities reflecting, e.g. a direction dependent heat conductivity. This enables an engineer to discretise larger portions of the device at hand because less mesh points have to be used in an averaged domain.

It was shown that a hierarchy of models can be set up for the simulation of fuel cells. The models of lower levels provide the effective parameters for the next higher level. It is furthermore possible to integrate experimental data at any stage into the model cascade, which either is used to validate the model or to input otherwise unknown model parameters. While the presented examples were taken from SOFC systems, the method applies to other types of fuel cells, such as PEFC as well.

4.2. Outlook

There is a lot more work to be done. On one hand, it is important to test the model hierarchies set-up with the NVAM for all interactions with independently measured experimental data. On the theoretical side, it is necessary to find rigorous proofs or estimates for the approximations made.

Furthermore, we are currently applying the NVAM to PEFC systems.

Acknowledgements

This work has been supported by the Swiss Commission for Technology and Innovation (CTI) under the Contract no. 5584.2.

References

[1] St. Whitaker, The Method of Volume Averaging, Kluwer Academic Publishers, Dordrecht, 1999.
[2] H. Brenner, D.A. Edward, Macro Transport Processes, Butterworth-Heinemann, Boston, 1993.
[3] W. Dong, G. Price, B. Wightman, D. Ghosh, M. Tabatabaian, Modelling of SOFC Stack and System Components, in: Proceedings of the Fifth European SOFC Forum, Luzern, 2002, pp. 929–936.
[4] T. Berning, D.M. Lu, N. Djilali, Three-dimensional computational analysis of transport phenomena in a PEM fuel cell, J. Power Sources 106 (2002) 284–294.
[5] R. Diethelm, E. Batawi, Status of the Sulzer HEXIS Product Development, in: Proceedings of the Fourth European SOFC Forum, Luzern, 2000, pp. 183–191.
[6] P. Costamagna, K. Honegger, Modelling of solid oxide heat exchanger integrated stacks and simulation at high fuel utilisation, J. Electrochem. Soc. 145 (11) (1998) 3995–4007.
[7] U. Harnisch, M. Roos, E. Batawi, Th. Baumgartner, A. Schuler, Numerical Simulation of HEXIS–SOFC Systems, in: Proceedings of the Fifth European SOFC Forum, Luzern, 2002, pp. 953–960.
[8] E. Achenbach, J. Power Sources 49 (1994) 333.
[9] E. Anderheggen, et al., NMSeses User Manual, Numerical Modelling GmbH, Thalwil, 2002.
[10] U. Bossel, Final Report on SOFC Data—Facts and Figures, IEA SOFC Task Report, Bern, 1992.